

# ChemComm

## Flowable Organic Slurry Battery with 1000 Cycles

Journal:	ChemComm
Manuscript ID	CC-COM-06-2024-003064.R3
Article Type:	Communication

SCHOLARONE™ Manuscripts

## ChemComm

#### COMMUNICATION

### Flowable Organic Slurry Battery with 1000 Cycles

Rajeev K. Gautam, Xiao Wang, Amir Lashgari and Jianbing "Jimmy" Jiang\*

Received 00th January 20xx, Accepted 00th January 20xx

DOI: 10.1039/x0xx000000x

We herein report a newly developed organic slurry flow battery. The strategically designed highly insoluble viologens (C8-V, C12-V, and C18-V) with two electron-activity were utilized to demonstrate a high energy density slurry battery with a stable capacity of 97%, power density of 123 mW/cm², and Coulombic efficiency over 99%.

Aqueous redox flow batteries (ARFBs) offer distinct advantages over non-aqueous RFBs, such as high ionic conductivity, low cost, high power density, and better safety. These systems have been extensively studied with both inorganic and organic redox compounds. Melanic redox materials provide better solubility and tunable redox potential, allowing for tailored molecular design. Melanic materials in conventional RFBs present challenges. Using insoluble materials as slurries can effectively address these solubility issues. Recently, semi-solid slurries of insoluble inorganic materials have emerged for highenergy density semi-solid flow batteries (Fig. S1). However, developing flowable slurries of organic redox-active materials remains challenging due to their lower volumetric energy density.

Viologen is a leading anolyte for ARFBs, offering two-electron activity, low cost, tunable structure, fast redox kinetics, high stability, and robust cycling performance. However, viologen-based ARFBs often struggle with stability due to dimerization of radical cations towards higher concentrations (> 1 M), limiting practical use. How to operate at 0.1 M to 0.5 M (Table S1), with only a few exploring higher concentrations over 100–200 cycles. Herein, we proposed a new organic slurry battery using two-electron active insoluble viologens with varying alkyl chains (C18-V, C12-V, and C8-V) as the high-energy density anolyte. Besides enhancing energy density, the slurry

configuration also addresses practical aspects like capacity fading from crossover and limited electrolyte solubility common in liquid flow batteries. The slurry batteries were tested under static and flow conditions using a single-channel cell with a syringe pump to ensure smooth slurry injection and prevent agglomeration. The organic slurry battery exhibited exceptional long-term stability and high efficiency in both static and flow configurations.

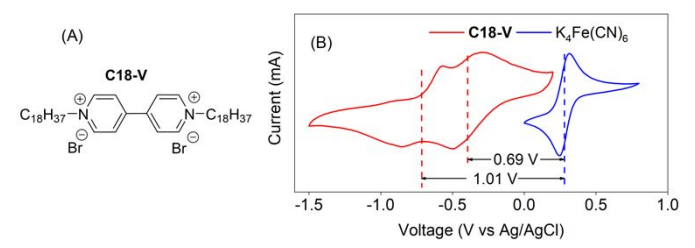


**Fig. 1** (A) chemical structure of **C18-V**. (B) Cyclic voltammograms of 0.1 M **C18-V** in 0.1 M KCl solution and 5.0 mM  $K_4$ Fe(CN)<sub>6</sub> at a scan rate of 50 mV/s.

Cyclic voltammetry (CV) study revealed two distinct singleelectron reductions at -0.41 V and -0.73 V vs. Ag/AgCl for C18-V (Fig. 1A). Unlike traditional redox flow batteries, where ions (such as Br<sup>-</sup>, Cl<sup>-</sup>) primarily serve to balance charge, here they also participate in the conversion from liquid-phase ions to a solid-state slurry. This transition facilitates intercalation reactions, leading to a significant peak-to-peak separation attributed to the intercalation/ deintercalation of ions (Cl-/Br-), similar to redox polymer.<sup>21,22</sup> The electrochemical reactions are most likely limited by transport of Cl-/Br-. Conversely, the K<sub>4</sub>Fe(CN)<sub>6</sub> aqueous catholyte exhibited a reversible oneelectron reduction at 0.28 V vs. Ag/AgCl in 0.1 M KCl. The halfbattery reaction of both C18-V anolyte and K<sub>4</sub>Fe(CN)<sub>6</sub> catholyte is depicted in Fig. S2. Based on the CV results, pairing the C18-V anolyte with the K<sub>4</sub>Fe(CN)<sub>6</sub> catholyte in a battery configuration could theoretically provide voltages of 0.76 V for the first electron and 1.18 V for the second electron.

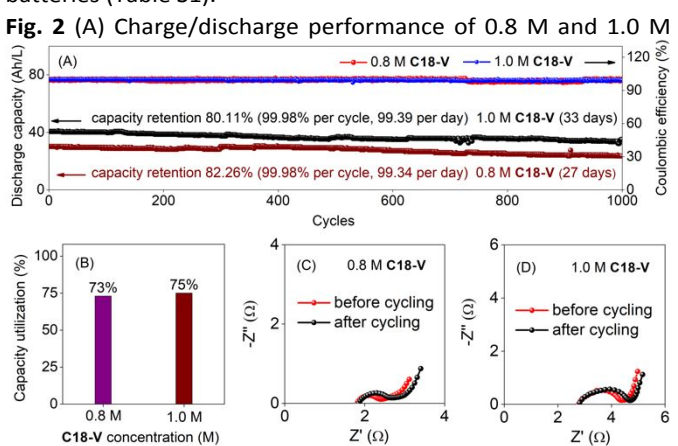
Department of Chemistry, University of Cincinnati, P.O. Box 210172, Cincinnati, Ohio 45221, USA. E-mail: <a href="mailto:jianbing.jiang@uc.edu">jianbing.jiang@uc.edu</a>

 $\mbox{\dag}$  Electronic supplementary information (ESI) available: See

DOI: 10.1039/x0xx00000x

COMMUNICATION ChemComm

Therefore, a static slurry battery was developed by pairing 0.8 M C18-V aqueous static slurry analyte with excess K<sub>4</sub>Fe(CN)<sub>6</sub>/K<sub>3</sub>Fe(CN)<sub>6</sub> (15 mL) flowing catholyte using an indigenously developed battery setup (Fig. S3A and S3B). Details of C18-V slurry preparation and Ketjen black (KB) optimization are provided in the ESI<sup>†</sup> and Fig. S4. The 0.8 M C18-V||K<sub>4</sub>Fe(CN)<sub>6</sub> static slurry battery was charged and discharged between 0 and 1.52 V at a current density of 10 mA/cm<sup>2</sup>. The long-term charge/discharge performance of the 0.8 M  ${\bf C18}$ -V| | K<sub>4</sub>Fe(CN)<sub>6</sub> static slurry battery is shown in Fig. 2A. The staticslurry battery exhibited a high discharge capacity of □31.2 Ah/L with retention of ~82% (99.98% per cycle, 99.34 per day) and Coulombic efficiency (CE) of over 99% for 1000 charge/discharge cycles (27 days). Furthermore, the battery exhibited a capacity utilization of 73% (Fig. 2B). The discharged capacity and long-term cycling stability of the 0.8 M C18- $V | | K_4Fe(CN)_6$  static slurry battery were notably higher compared to that of the reported viologen-based redox flow batteries (Table S1). 15,17-20,23-33



**C18-V**|| $K_4$ Fe(CN) $_6$  static slurry batteries. (B) Capacity utilization of 0.8 M and 1.0 M **C18-V**|| $K_4$ Fe(CN) $_6$  static slurry batteries. (C) EIS spectra of 0.8 M and 1.0 M **C18-V**|| $K_4$ Fe(CN) $_6$  static slurry battery before and after cycling.

In addition, a slurry battery with a higher concentration of 1.0 M C18-V (Fig. 2A) was assembled and tested under identical cycling conditions to study the effects of C18-V concentration on battery performance. The 1.0 M C18-V | K<sub>4</sub>Fe(CN)<sub>6</sub> static slurry battery demonstrated excellent long-term cycling performance, maintaining capacity retention of ~80% (99.98 per cycle, 98.39 per day) and CE of over 99% during 1000 charge/discharge cycles (33 days). Furthermore, demonstrated a discharge capacity of ~40.6 Ah/L with a theoretical capacity utilization of 75% (Fig. 2B), higher than that of the 0.8 M C18-V/K<sub>4</sub>Fe(CN)<sub>6</sub> battery. The charge and discharge plateaus observed at different cycling stages (Fig. S5) confirm that C18-V remains consistently active with two electrons. Furthermore, the 0.8 M and 1.0 M C18-V | K<sub>4</sub>Fe(CN)<sub>6</sub> static slurry batteries were characterized using EIS before and after cycling. The post-cycling batteries exhibited slightly higher Rct values (Fig. 2C and 2D). This reduction in kinetics during prolonged cycling may contribute to capacity fading for both the slurry batteries. Factors such as unidentified phase separation

of slurry constituents (C18-V and KB), membrane deactivation, and electrolyte degradation may contribute to this effect. To gain more information, the pre-and post-cycling slurries were examined through scanning electron microscopy (SEM) and energy dispersive spectroscopy (EDS) to observe a modification in the surface morphology and elemental composition, respectively. SEM images of C18-V (Fig. S6A), KB (Fig. S6B), and pre-and post-cycled C18-V slurries of different concentrations are shown in Fig. S6. Post-cycled battery slurries for 0.8 M C18-V (Fig. S6C and S6D) and 1.0 M C18-V (Fig. S6E and S6F) do not exhibit any obvious change in the microstructure, suggesting that the slurries of both batteries remained intact throughout the charge/discharge process. Moreover, EDS analysis (Fig. S7A-S7F) displays the uniform distribution of slurry constituents without any aggregation, further indicating the microstructural stability of 1.0 M C18-V slurry. Furthermore, the X-ray diffraction (XRD) characterization of the post-cycling slurry displayed no additional characteristic peaks (Fig. S8), confirming the high stability of the battery slurry. Moreover, the XRD characterization of the pre-and post-cycled battery membrane shows no evidence of crossover or absorption of carbon black or other species (Fig. S9)

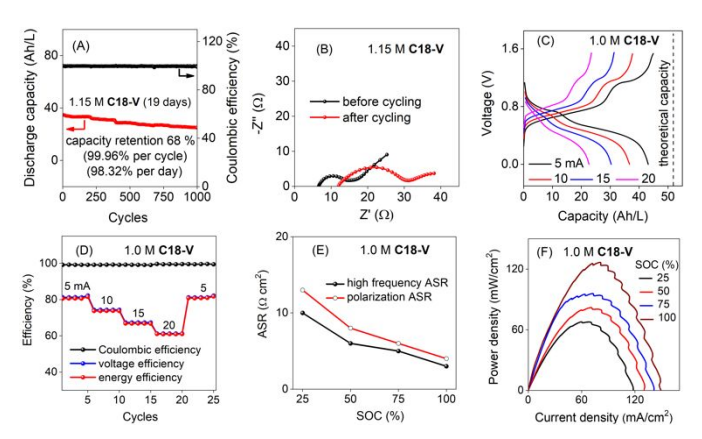


Fig. 3 (A) Charge/discharge performance of 1.15 M C18-V|| $K_4Fe(CN)_6$  static slurry battery. (B) EIS spectra of 1.15 M C18-V|| $K_4Fe(CN)_6$  static slurry battery before and after cycling. (C) Charge rate performance 1.0 M C18-V|| $K_4Fe(CN)_6$  static slurry battery. (D) Variation in CE, VE, and EE of 1.0 M C18-V|| $K_4Fe(CN)_6$  static slurry battery with varied current (electrode area of 1 cm²). (E) ASR and polarization behavior of 1.0 M C18-V|| $K_4Fe(CN)_6$  static slurry battery at varied SOCs. (F) Power density curve of 1.0 M C18-V|| $K_4Fe(CN)_6$  static slurry battery at varied SOCs.

To further enhance the energy density, a slurry battery with 1.15 M C18-V was assembled and subjected to testing under identical conditions Fig. 3. The 1.15M C18-V||K<sub>4</sub>Fe(CN)<sub>6</sub> static-slurry battery maintained capacity retention of 68% (99.96 per cycle, 97.53 per day) with a theoretical capacity utilization (52%) and CE of over 99% during 1000 charge/discharge cycles (~19 days) (Fig. 3A). However, both capacity retention (68%) and theoretical capacity utilization (52%) values were found to be lower compared to both 0.8 M C18-V and 1.0 M C18-V slurry batteries. To understand the mechanisms driving the

Journal Name COMMUNICATION

substantial decline in capacity retention and utilization at the higher concentration of 1.15 M C18-V, it is crucial to investigate the underlying factors. Hence, the pre- and post-cycled slurry batteries were analyzed using EIS and SEM analysis. Interestingly, the post-cycled slurry battery EIS revealed higher Rs and Rct (Fig. 3B) compared to the pre-cycled slurry battery. In addition, the impedance of the 1.15 M C18-V slurry battery was higher than that of both 0.8 M C18-V (Fig. 2C) and 1.0 M C18-V (Fig. 2D) static slurry batteries. These increased values of Rs and Rct, suggest poor kinetics of 1.15 M C18-V slurry. At higher concentrations (1.15 M), the incomplete wetting of all C18-V molecules by the inadequately available supporting electrolyte and KB particles occurs, leading to the inactivation of some viologen molecules and significant transport losses during battery cycling. Furthermore, the evident uneven distribution or aggregation of C18-V particles in the slurry (Fig. S6G and S6H) could lead to the phase separation issue. Consequently, the 1.15 M C18-V||K<sub>4</sub>Fe(CN)<sub>6</sub> static-slurry battery demonstrates poor capacity retention and low-capacity utilization.

The best-suited 1.0 M C18-V||K<sub>4</sub>Fe(CN)<sub>6</sub> static-slurry battery was further investigated for rate ability tests by varying the current density from 5 to 20 mA/cm<sup>2</sup> and the corresponding change in CE, voltage efficiency (VE), energy efficiency (EE), and the discharge capacity was measured for an average of five cycles. The battery displays a high capacity of 43.3 Ah/L at a low current density of 5 mA/cm<sup>2</sup> (Fig. 3C), which is close to 81% of the theoretical capacity. Even at a high discharge current density of 20 mA/cm<sup>2</sup>, the battery delivers a capacity of 22.7 Ah/L, which is extremely high compared to the reported viologen-based batteries (Table S1).15,17-20,23-33 As the applied current density increases from 5 to 20 mA/cm<sup>2</sup>, there is a noticeable decrease in discharge capacity (Fig. 3C), VE, and EE (Fig. 4D) due to increased mass transport losses, which causes higher overpotential. Consequently, both VE and EE decrease from 81.14% and 80.52% to 61.5% and 60.45%, respectively, as current density increases from 5 to 20 mA/cm<sup>2</sup>. Interestingly, CE remains stable at over 99% across all current densities, demonstrating that no side reactions occur in the slurry battery. When cycled back to the low current density of 5 mA/cm<sup>2</sup>, the static slurry battery successfully regains its original VE and EE values, showcasing its excellent charge-rate capability. Furthermore, the power density and polarization performance of the 1.0 M C18-V | | K<sub>4</sub>Fe(CN)<sub>6</sub> static slurry battery were also measured to assess the electrochemical performance of slurry batteries under various state of charge (SOC) conditions. In addition, the area-specific resistance (ASR) data for both electrolyte resistance and total cell resistance under static conditions were examined. The results indicate that both the ASR of the electrolyte and the total cell increase with increasing SOC (Fig. 3E). However, the electrolyte resistance constitutes over 77% of the total cell resistance for all batteries. The polarization curves of the 1M C18-V | K<sub>4</sub>Fe(CN)<sub>6</sub> static slurry battery (Fig. 3F) indicate that both peak power density and current density increase with the SOC of the battery, demonstrating stable charge/discharge of the battery. The C18- $V||K_4Fe(CN)_6|$  battery exhibits a peak power density of 123

mW/cm². In addition to C18-V, a 1.0 M C12-V| $K_4$ Fe(CN)<sub>6</sub> static battery was also assembled and demonstrated for long-term charge/discharge performance (Fig. S10). However, the 1.0 M C12-V| $K_4$ Fe(CN)<sub>6</sub> slurry battery exhibited poor performance compared to the 1.0 M C18-V| $K_4$ Fe(CN)<sub>6</sub> slurry battery, showing significant capacity fade after 65 cycles. The 1.0 M C12-V| $K_4$ Fe(CN)<sub>6</sub> static slurry battery demonstrated capacity retention of 34% for 380 charge/discharge cycles with a CE of over 99% (Fig. S10). The rapid capacity fading could be ascribed to the shorter alkyl chains of C12-V, which could not hold the phase separation of composite slurry constituents.

The static-slurry batteries with varying C18-V concentrations show promise for energy storage but are limited by their inability to independently scale energy and power. Transitioning to a slurry flow battery configuration could address this by combining the high energy density of static batteries with the scalability of conventional RFBs. Slurry flow batteries were developed using flowable C18-V slurry analytes (0.5 M and 0.7 M) paired with a K<sub>4</sub>Fe(CN)<sub>6</sub> catholyte. Figures S11A and S11B show the slurries, while Fig. S11C illustrates the setup with two injection pumps for the flow of concentrated organic slurry.

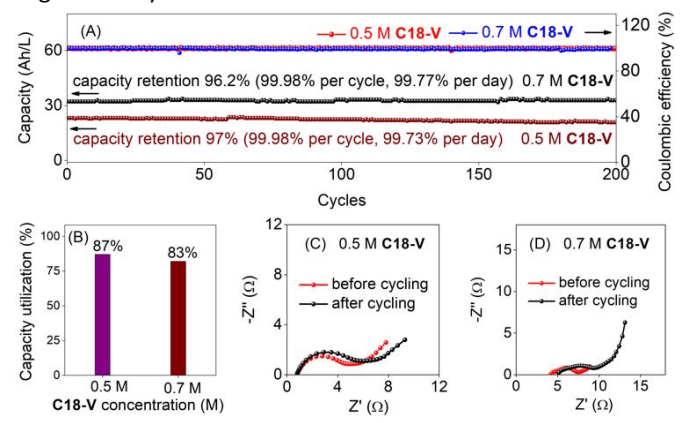


**Fig. 4** (A) Charge/discharge performance of 0.5 M and 0.7 M **C18-V** $|K_4Fe(CN)_6$  flow slurry batteries. (B) Capacity utilization of 0.5 M and 0.7 M **C18-V** $|K_4Fe(CN)_6$  flow slurry batteries. discharge capacity and Coulombic efficiency over 1000 cycles. Electrochemical impedance spectra (EIS) before and after cycling of 0.5 M and 0.7 M **C18-V** $|K_4Fe(CN)_6$  slurry flow battery.

The slurry flow rate is crucial for optimal battery capacity at a given charge/discharge current. It was optimized by testing the performance of the slurry flow battery at flow rates of 0.1, 0.2, and 0.4 mL/min using 0.7 M C18-V slurry at 10 mA/cm² (Fig. S11D). The battery performed best at 0.2 mL/min, which was used in subsequent studies. A 0.5 M C18-V |  $K_4$ Fe(CN)<sub>6</sub> slurry flow battery was cycled for 200 charge/discharge cycles (Fig. 4A), achieving high cycling stability with 97.12% capacity retention (99.98% per cycle, 99.73% per day), CE close to 100%, and EE of 71%. The successful demonstration of the 0.5 M C18-V |  $K_4$ Fe(CN)<sub>6</sub> slurry flow battery inspired further investigation with a higher concentration of 0.7 M C18-V slurry. This new battery was cycled for 200 cycles (Fig. 4A), achieving a capacity retention of 96.23% (99.98% per cycle, 99.77% per day), CE over

COMMUNICATION ChemComm

99%, and EE of 69%. Capacity utilization was 83%, slightly lower than the 87% from the 0.5 M slurry (Fig. 4B). The charge/discharge profile indicated consistent two-electron utilization (Fig. S12), and EIS results showed minimal impedance changes, indicating stable kinetics (Fig. 4C and 4D). A 1.0 M C18-V|| $K_4$ Fe(CN) $_6$  slurry flow battery was assembled but performed poorly due to high viscosity.

While the C18-V slurry batteries show promise, several challenges remain to be addressed. First, mechanism of the electrochemical reaction. Due to the difficulty of conducting cyclic voltammetry experiments in slurry systems, we have yet to determine the specific control mechanism of the electrochemical reactions, whether they are diffusioncontrolled, electrochemically controlled, or a mixed process. Our findings suggest that the reaction is likely constrained by the transport of Br<sup>-</sup>/Cl<sup>-</sup> within the C18-V phase or by the underlying electrochemical kinetics. However, this aspect is not the primary focus of the current study, more comprehensive discussion on this topic can be found in the work by Yoon et al.<sup>22</sup> Second, consideration of counter-ions in the slurry system. Unlike traditional flow batteries, where the redox-active species are dissolved in the electrolyte, the slurry system remains in a solid-state before and after the reaction. This introduces the need to account for the transition of counter-ions from solution to solid-state, which could be the rate-limiting step of the entire reaction, thus affecting the overall battery performance. Third, design of a continuous injection pump system: The current flow system employs an injection pump for flow control, which does not provide continuous flow. This indicates that the chargedischarge cycles need to be synchronized with the slurry flow rate, adding complexity to the system.

In summary, organic slurry batteries employing strategically designed two-electron active insoluble viologens (Cn-V) with varying alkyl chain lengths were successfully demonstrated. The organic slurry with optimal electroactive properties was developed and evaluated across different concentrations of C18-V in the slurry batteries under both static and flow configurations. The slurry batteries maintained 80% capacity after 1000 cycles in static and 97% after 200 cycles in flow conditions. Both slurry configurations showed Coulombic efficiency exceeding 99%. This approach represents a viable way for high-energy-density storage systems based on insoluble redox materials.

This study was supported by the National Science Foundation under grant no. CBET-2112798.

#### Data availability

The data supporting this article have been included as part of the ESI. †

#### **Conflicts of interest**

There are no conflicts to declare.

#### Notes and references

1. S. Gentil, D. Reynard and H. H. Girault, *Curr. Opin. Electrochem.*, 2020, **21**, 7–13.

- 2. R. K. Emmett and M. E. Roberts, *J. Power Sources*, 2021, **506**. 230087.
- 3. J. Winsberg, T. Hagemann, T. Janoschka, M. D. Hager and U. S. Schubert, *Angew. Chem. Int. Ed.*, 2017, **56**, 686–711.
- 4. D. Chao, W. Zhou, F. Xie, C. Ye, H. Li, M. Jaroniec and S.-Z. Qiao, *Sci. Adv.*, 2020, **6**, eaba4098.
- 5. Y. Liu, Q. Chen, P. Sun, Y. Li, Z. Yang and T. Xu, *Mater. Today Energy*, 2021, **20**, 100634.
- 6. J. Luo, A. P. Wang, M. Hu and T. L. Liu, *MRS Energy & Sustain.*, 2022, **9**, 1–12.
- 7. N. Aguilo-Aguayo, D. Hubmann, F. U. Khan, S. Arzbacher and T. Bechtold, *Sci. Rep.*, 2020, **10**, 5565.
- 8. F. Soavi, A. Brilloni, F. De Giorgio and F. Poli, *Curr. Opin. Chem. Eng.*, 2022, **37**. 100835.
- 9. M. Duduta, B. Ho, V. C. Wood, P. Limthongkul, V. E. Brunini, W. C. Carter and Y. M. Chiang, *Adv. Energy Mater.*, 2011, **1**, 511–516.
- 10. F. Y. Fan, W. H. Woodford, Z. Li, N. Baram, K. C. Smith, W. C. Carter and Y. M. Chiang, *Nano Lett.*, 2014, **14**, 2210–2218.
- 11. C. Wang, Q. Lai, P. Xu, X. Li and H. Zhang, *Chin. Chem. Lett.*, 2018, **29**. 716–718.
- 12. S. Cheng, Y. Hu, L. Jiang, H. Dang, Y. Ding, Q. Duan, H. Xiao, J. Sun and Q. Wang, *Fire Technol.*, 2022, **59**, 1181–1197.
- 13. W. Yan, C. Wang, J. Tian, G. Zhu, L. Ma, Y. Wang, R. Chen, Y. Hu, L. Wang, T. Chen, J. Ma and Z. Jin, *Nat. Commun.*, 2019, **10**, 2513.
- 14. M. Chen, L. Liu, P. Zhang and H. Chen, RSC Adv., 2021, 11, 24429.
- 15. C. DeBruler, B. Hu, J. Moss, X. Liu, J. Luo, Y. Sun and T. L. Liu, *Chem*, 2017, **3**, 961–978.
- 16. B. Hu, Y. Tang, J. Luo, G. Grove, Y. Guo and T. L. Liu, *Chem. Commun.*, 2018, **54**, 6871–6874.
- 17. L. Liu, Y. Yao, Z. Wang and Y. C. Lu, *Nano Energy*, 2021, **84**, 105897.
- 18. B. Hu, H. Fan, H. Li, M. Ravivarma and J. Song, *Adv. Funct. Mater.*, 2021, **31**, 2102734.
- 19. T. Janoschka, N. Martin, M. D. Hager and U. S. Schubert, *Angew. Chem. Int. Ed.*, 2016, **55**, 14427–14430.
- 20. S. Jin, E. M. Fell, L. Vina-Lopez, Y. Jing, P. W. Michalak, R. G. Gordon and M. J. Aziz, *Adv. Energy Mater.*, 2020, **10**, 2000100.
- 21. A. Sargent, T. Loi, S. Gal and O. A. Sadik, *J. Electroanal. Chem.*, 1999, **470**, 144–156.
- 22. T.-H. Le, Y. Kim and H. Yoon, Polymers, 2017, 9, 150.
- 23. J. Luo, B. Hu, C. Debruler and T. L. Liu, *Angew. Chem.*, 2018, **130**, 237–241.
- 24. H. Wang, D. Li, J. Xu, Y. Wu, Y. Cui and L. Chen, *J. Power Sources*, 2021, **492**, 229659.
- 25. B. Hu and T. L. Liu, J. Energy Chem., 2018, 27, 1326–1332.
- 26. S. Liu, M. Zhou, T. Ma, J. Liu, Q. Zhang, Z. Tao and J. Liang, *Chin. Chem. Lett.*, 2020, **31**, 1690–1693.
- 27. C. DeBruler, B. Hu, J. Moss, J. Luo and T. L. Liu, *ACS Energy Lett.*, 2018. **3**. 663–668.
- 28. H. Li, H. Fan, B. Hu, L. Hu, G. Chang and J. Song, *Angew. Chem. Int. Ed.*, 2021, **60**, 26971–26977.
- 29. W. Wu, J. Luo, F. Wang, B. Yuan and T. L. Liu, *ACS Energy Lett.*, 2021, **6**, 2891–2897.
- 30. M. Pan, L. Gao, J. Liang, P. Zhang, S. Lu, Y. Lu, J. Ma and Z. Jin, *Adv. Energy Mater.*, 2022, **12**, 2103478.
- 31. B. Hu, Y. Tang, J. Luo, G. Grove, Y. Guo and T. L. Liu, *Chem. Commun.*, 2018, **54**, 6871–6874.
- 32. W. Liu, Y. Liu, H. Zhang, C. Xie, L. Shi, Y. G. Zhou and X. Li, *Chem. Commun.*, 2019, **55**, 4801–4804.
- 33. T. Hagemann, J. Winsberg, M. Grube, I. Nischang, T. Janoschka, N. Martin, M. D. Hager and U. S. Schubert, *J. Power Sources*, 2018, **378**, 546–554.

Page 5 of 5 ChemComm

## Data availability

The data supporting this article have been included as part of the ESI.†